Electrical and photovoltaic properties of self-assembled Ge nanodomes on Si(001)

M. Kratzer,[1] M. Rubezhanska,[2] C. Prehal,[1] I. Beinik,[1] S. V. Kondratenko,[3] Yu. N. Kozyrev,[2] and C. Teichert[1,*]

[1]*Institute of Physics, Montanuniversität Leoben, Franz Josef Str. 18, A-8700 Leoben, Austria*

[2]*O.O. Chuiko Institute of Surface Chemistry, 17 Generala Naumova Str. 03164, Kiev, Ukraine*

[3]*National Taras Shevchenko University, Physics Department, 2 Acad. Glushkov Ave, UA-03022, Kiev, Ukraine*

(Received 3 August 2012; revised manuscript received 30 November 2012; published 26 December 2012)

SiGe nano-size islands play a key role in novel electronic and optoelectronic devices. Therefore, the understanding of basic electrical properties of individual nanoislands is crucial. Here, the electrical and photovoltaic properties of individual self-assembled Ge nanodomes (NDs) on Si(001) have been studied by conductive and photoconductive atomic force microscopy (AFM). The transition areas between the {113} and {15 3 23} facets turned out to be most conductive whereas the {113} facets exhibit minimum conductivity, which is attributed to a local increase in Si concentration. Local current-to-voltage measurements revealed that the NDs show an ohmic resistance, which is in the MΩ region and scales with the ND-substrate interface area. Upon illumination by the AFM feedback laser at 860 nm, a photovoltage is generated. This photovoltage originates in the *p*-*i*-*n* structure formed between the *p*-type substrate, the Ge ND, and the *n*-type diamond AFM probe.

DOI: 10.1103/PhysRevB.86.245320 PACS number(s): 73.40.−c, 73.63.Bd, 73.50.Pz

I. INTRODUCTION

The Ge/Si(001) system is an intensively studied model system for lattice mismatched semiconductor nanostructures. Deposition of Ge or SiGe on a silicon substrate yields the spontaneous formation of three-dimensional (3D) crystallites in order to release misfit strain energy at the cost of a surface energy increase when a critical layer thickness is exceeded.[1] Morphology, nucleation, shape evolution, and alloying of these self-assembled Ge (or SiGe) islands on Si(001) have been subject to detailed investigations.[1–3] Depending on the growth conditions and the amount of deposited Ge, 3D islands with different geometries evolve: hut clusters, pyramids, domes, and barns.[4–9] As prototype system for the investigation of Stransky-Krastanow growth, it is also important as a model system for semiconductor heterostructures, which are of great significance in the development of electronic and optoelectronic devices. Especially the potential for the utilization of the latter mentioned nanostructures for the fabrication of heterodevices compatible with Si-based technology appeals the interest of researchers and engineers.[10–12] Possible applications range from strain-engineered high mobility field effect transistors[13,14] to infrared photodetectors.[15,16] With this respect, the lateral alignment of SiGe nanostructures has been and still is extensively studied. Island ordering can be realized via self-assembling due to elastic interaction of neighboring islands or due to deposition on prepatterned surfaces.[1,17–22] Also, 3D stacking of SiGe nanodot layers has been realized. [2,23–25] In view of the possible application in electronics, the electrical and optical properties of building blocks made of SiGe two-dimensional (2D) arrays and 3D-stacks have been studied.[16,26–28] To gain more insight into the electrical, optoelectronic, and photovoltaic behavior of Ge (SiGe) nanoisland-containing devices, detailed knowledge of the properties of individual islands is necessary. However, studies on the electrical behavior of individual Ge (SiGe) nanofacetted crystallites are rare.[29–32] Especially for devices based on a few or even single crystallites, detailed knowledge about local differences in the electrical behavior within a single crystallite is crucial. In this work, we have applied conductive atomic force microscopy (C-AFM)[33–35] and photoconductive AFM (PC-AFM)[36] in order to characterize the current and photocurrent transport through individual self-assembled Ge crystallites on Si(001) with the focus on multifaceted Ge crystallites, so called nanodomes (NDs).[4,9] The aim was to extract the influence of geometrical ND properties on the electrical and photoelectrical properties. We especially concentrated our study on the facet type and ND size. 2D current maps show an inhomogeneous current distribution over the NDs related to the facet structure. Local current-to-voltage (IV) measurements of the center of individual NDs in the dark and under illumination yield the generation of a photovoltage and a size-dependent short circuit current, which is related to the ND ohmic resistance.

II. EXPERIMENTAL

Ge NDs were fabricated using molecular beam epitaxy (MBE) under ultrahigh vacuum conditions. As substrate a 4-inch p-Si(001) wafer, boron doped (doping level $N_A \sim 10^{15}$ cm^{-3}), with a miscut angle smaller than a few tenths of a degree, was used. For deposition monitoring, reflection high energy electron diffraction (RHEED) was employed. After oxide removal, a well-defined Si(001) surface was achieved by depositing a Si buffer layer onto the silicon wafer substrate until a high contrast Si(001) 2×1 electron diffraction pattern was visible. Subsequently, Ge was deposited at a deposition rate of ∼0.05 Å/s and a substrate temperature of 600° C, resulting in a strain-driven formation of Ge NDs with lateral extensions between 60 and 450 nm.[37]

For the AFM measurements, 1×1 cm^2 samples were cut out of the center region of the 4-inch wafer. For electrical characterization, the wafer pieces were contacted with a drop of silver paint at the back. In order to avoid the disturbing influence of the silicon oxide on the contact, the oxide was removed by scratching the silver paint-covered sample while the silver paint was still liquid. The AFM measurements were performed with an Asylum Research MFP-3D system equipped with an 80×80 μm$^2 \times 15$ μm closed loop

scanner and an 860 nm super luminescent diode (SLD) for readout of the cantilever bending. The high resolution morphological characterization was performed by intermittent contact mode (tapping mode, TM) measurements using HiRes 150 AFM probes from Budged Sensors with a typical cantilever resonance frequency of 150 kHz and a tip curvature radius <1 nm. C-AFM and PC-AFM, both operating in contact mode, were employed under ambient conditions. For C-AFM and PC-AFM measurements nitrogen-doped diamond-coated conductive probes (DCP-11 from NT-MDT) were used. For the current images, the bias was applied to the sample via the silver back contact while the tip stayed grounded. 2D current maps with simultaneous topography acquisition were always recorded under illumination by the SLD of the optical AFM feedback. For recording dark current maps, the SLD has to be switched off. Before switching off the SLD, the tip was brought to contact with the surface, and then the feedback gains were set to zero. In this mode, which is similar to a constant height mode, no topography acquisition is possible in contrast to standard contact mode measurements with activated feedback, which corresponds to constant force mode measurements. Local current-to-voltage (IV) curves were measured on single NDs in the dark and under illumination. The IV curves were recorded by positioning the conductive AFM tip on top of the center region of a selected ND. Then a voltage ramp between ± 2 V was applied to the sample at a rate of 4 V/s. For better data statistics, eight full IV curves were measured at each point and averaged.

III. RESULTS

A. Morphology and 2D current maps

In Figs. 1(a) and 1(b), the topography image of the as prepared Ge ND/Si(001) sample and the corresponding current map (sample bias -0.2 V) recorded simultaneously in contact mode are depicted. Compared to conventional intermittent contact (tapping) mode imaging, the image quality is rather low due to the increased forces acting on the tip in contact mode. The NDs are clearly visible as bright almost circular dots in the image. Since the structures deviate—depending on their size—more or less from the circular shape, it is advantageous to express the dome size in terms of an effective diameter. The effective diameter refers to a circular disk with an area equal to the projected ND area. A histogram of the corresponding effective dot sizes is presented in the inset of Fig. 1(a). It results from an automatic evaluation of 718 objects performed by the scanning probe microscopy visualization and analysis software Gwyddion.[38] The evaluation yields that the majority of the NDs exhibit effective diameters larger than 100 nm. In fact, a significant number of structures smaller than that can be found on the surface, but the software does not adequately identify them. We focus here on objects with effective diameters larger than 50 nm because there the individual facets were easily distinguishable in both topography and current image, enabling a proper attribution. The ND density determined from Fig. 1(a) is 6.5 NDs/μm^2 and is representative for the whole sample area investigated.

In the current image presented in Fig. 1(b), the dark regions represent areas of higher current and the bright areas represent

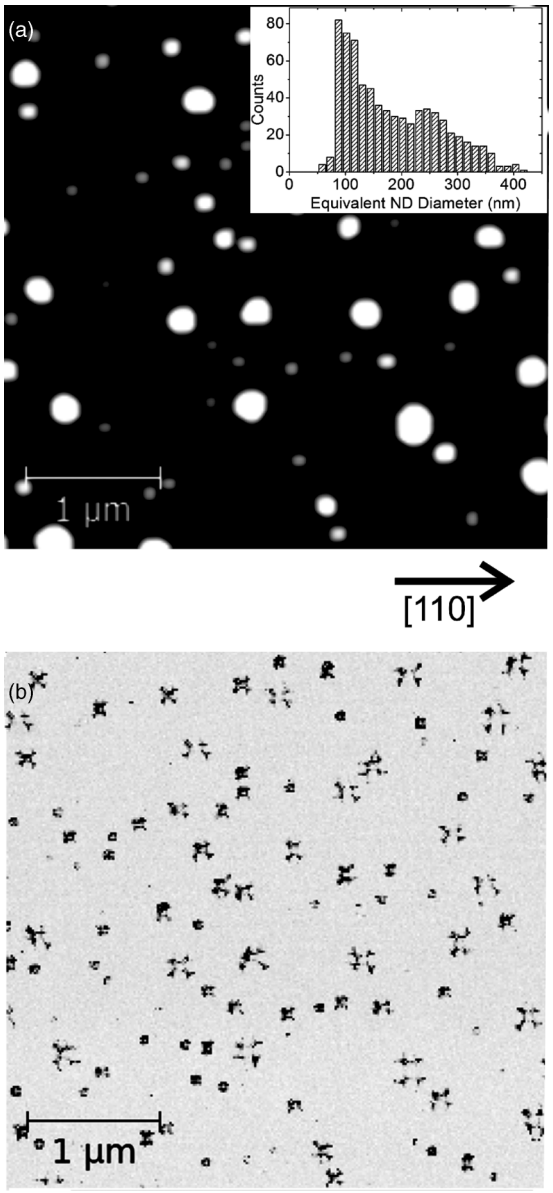

FIG. 1. (a) 4×4 μm^2 contact mode topography image of Ge nanodomes on a Si(001) substrate (z scale $=$ 100 nm) and the corresponding current image (b) measured under illumination at a sample bias of -0.2 V (dark areas mean high current, current scale -10 nA). The inset in (a) shows a histogram of the dome size distribution.

almost nonconductive regions. The maximum current obtained under the applied conditions is about -9 nA. Thus, we can state that the 3D Ge crystallites show a significantly higher conductivity than the surrounding wetting layer. Even shallow structures that are not well visible in the topography image can be distinguished from the less conductive ($\sim$2 pA) wetting layer. It is remarkable that the current from the NDs show a clear fine structure, which is obviously related to the nanofacetted slope of the NDs.

In order to clarify the NDs 3D facet structure, we performed high-resolution TM AFM measurements presented in Fig. 2, which revealed clearly that the NDs exhibit well-oriented facets. An analysis of the facets in terms of frequency

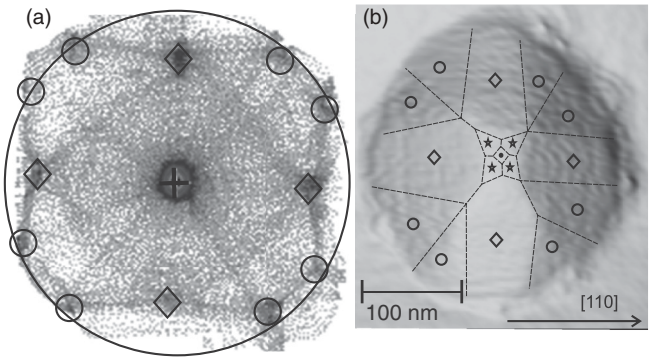

FIG. 2. (a) Result of a facet analysis (frequency of occurrence and orientation of planes with their angular orientation with respect to the surface normal) calculated from a 1.5×1.5 μm^2 tapping mode AFM image. The big black circle is marking a polar angle of 35°. The facets are indicated by open diamonds ({113}) and circles ({15 3 23}). (b) Intermittent contact mode AFM image of a single Ge ND on Si(001) in 3D presentation with assignment of the facets ($\star${105}, •{001}, ◊{113}, ○{15 3 23}).

and angular orientation with respect to the surface normal (also performed by Gwyddion) is depicted in Fig. 2(a). The central dark spot indicates the (001) plane and accordingly corresponds to the surface of the wetting layer covered Si substrate and to the (001) top faces of the NDs. The off-center spots have polar angles of $(36 \pm 3)^\circ$ and $(28 \pm 3)^\circ$, respectively, and appear at azimuthal angles of $(34 \pm 3)^\circ$ and $(0 \pm 3)^\circ$ with respect to the [110] direction. Thus, they can be attributed to {15 3 23} and {113} facets, respectively.[4,9] In Fig. 2(b), the {113} and {15 3 23} facets are indicated together with the {105} and {001} facets at the top of the domes. The center (001) facet surrounded by the four {105} facets is not detected in the facet analysis, but the diamondlike shape at the ND top is characteristic for these features. The spots corresponding to the {15 3 23} facets in Fig. 2(a) appear sometimes smeared out towards a bit larger angles, which we interpret as the onset of {20 4 23} facets,[4,9] indicating that the larger NDs are at the transition from the dome state to the barn state.[9]

For a clear correlation of the current distribution of the domes with their facet structure, a current map was measured at higher precision with the results presented in Fig. 3. Figures 3(a) and 3(b) are the simultaneously measured topography and current image of a 1×1 μm^2 area at 0 V sample bias in trace direction. Interestingly, maximum currents up to −9 nA are detectable even though the sample is unbiased. The current maxima in Fig. 3(b) appear preferentially at the transition between the facets, whereas there is almost no current from the larger side facets. The relative increase in current measured at the bottom right part of the domes is also present in the retrace images (see inset), which excludes an influence due to different contact forces when scanning ascending and descending slopes of the islands. Therefore, the systematic left-right difference is most likely due to an asymmetry of the tip's conductive coating. Figure 3(c) shows a current image of the same area for a sample bias of −0.5 V. Additionally, the feedback SLD was switched off in order to elucidate the influence of light on the current

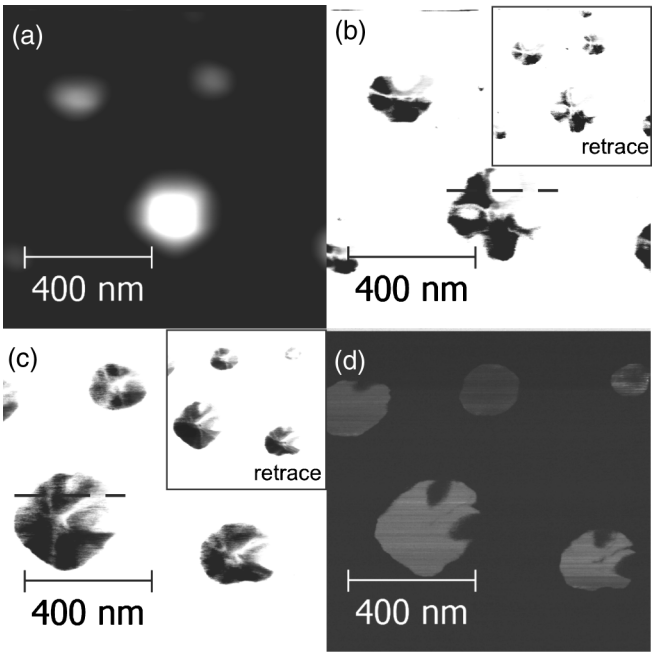

FIG. 3. (a) Contact mode topography image of a 1×1 μm^2 sample area (z scale = 60 nm). The corresponding current images under illumination (860 nm) at 0 V bias (b) and in the dark at −0.5 V bias (c). Dark areas mean higher currents, current scale −5 nA. (d) Dark current image of approximately the same area at nominally 0 V applied bias (current scale −8 pA). The lateral shift in (c) and (d) is mainly caused by thermal drift effects. The insets in (b) and (c) are the corresponding retrace current images for comparison.

image. Since the SLD was switched off, the measurement was done without feedback. Note that the image is left-shifted by a few 100 nm compared to Figs. 3(a) and 3(b), which is mainly due to thermal drift effects and the lack of feedback control. In this case, the maximum currents also reach about −9 nA. Comparing Figs. 3(b) and 3(c), it is clear that in the dark case not only the transition between the facets [as in Fig. 3(a)] but also the larger side facets exhibit considerable conductivity. A comparison of the current profiles in Fig. 4, which were taken along the dashed lines in Figs. 3(b) and

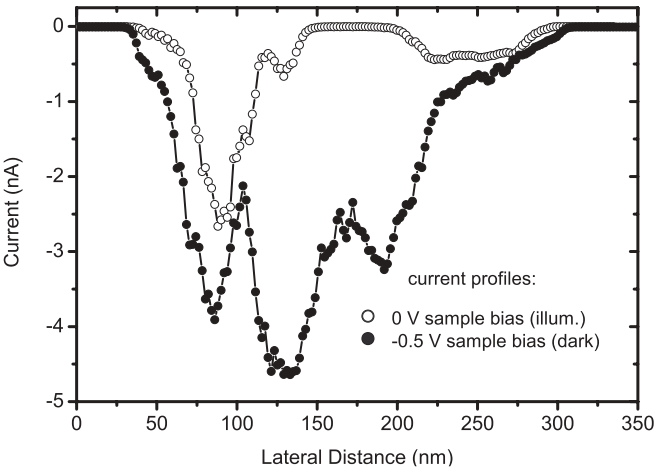

FIG. 4. Current profiles recorded along the dashed lines in Fig. 3(b).

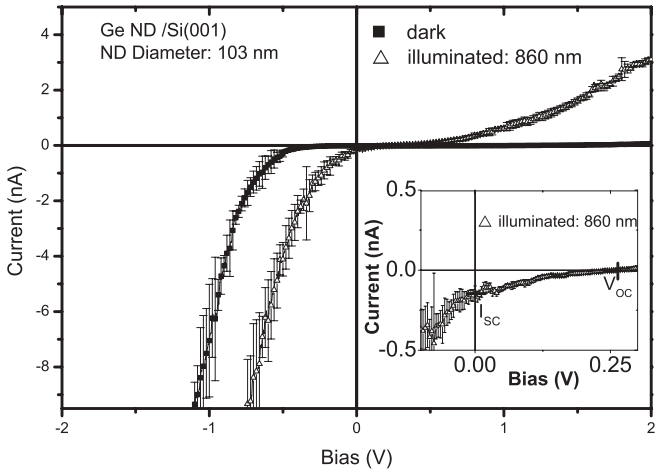

FIG. 5. Current-to-voltage characteristics measured on top of a single Ge nanodome with a diameter of about 100 nm in the dark (black squares) and under illumination (white triangles). The inset presents the low positive bias region under illumination with enlarged scale.

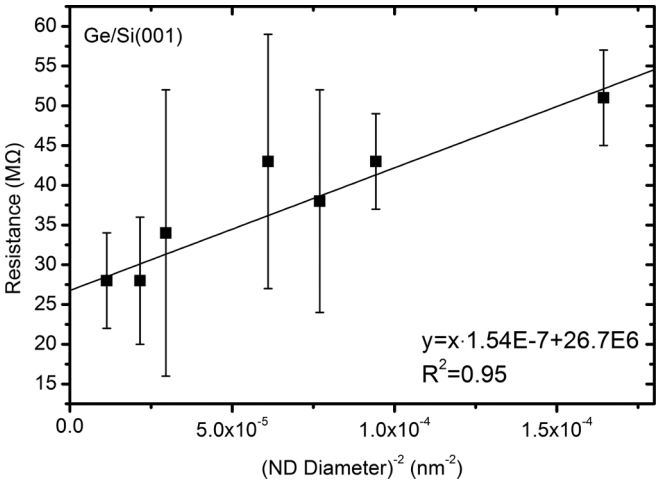

FIG. 6. Ohmic resistance determined from the IV curves of various nanodomes plotted versus the reciprocal square of the nanodome diameter. The full straight line is a linear regression to the data. The corresponding equation and the coefficient of determination are given in the right bottom corner.

3(c), confirms the latter observation. Both current profiles exhibit analog behavior along the first 100 nm on the left and the last 100 nm on the right but differ significantly between 100 and 250 nm. In this region, the dark current reaches values up to −4.5 nA, whereas almost zero current is observed for the unbiased case under illumination. In Fig. 3(d), a further current image is presented with 0 V bias and without illumination by the SLD light. In this case, the maximum current is ∼−7.5 pA and is measured on the substrate whereas the current from the domes is ∼4 pA. The change in contrast at the top 200 nm was caused by a tip change due to sudden damage, which is a frequently occurring problem when scanning without feedback control. Also, the occurrence of identical features at the right side of the two bottom islands confirms that the tip was slightly damaged.

B. Local IV characteristics

In Fig. 5, an example for IV curves for the dark and the illuminated case measured at the center of a 103-nm diameter ND is depicted. The positive bias corresponds to a positive potential applied to the Ag back electrode of the sample. In the dark case, significant current sets on at around −0.5 V, whereas the breakdown at positive bias is not reached within the applied voltage range. In the illuminated case where the sample stays under illumination by the AFM feedback SLD at 860 nm, the IV curve changes significantly. First, there is a significant current at positive biases higher than +0.5 V. Second, the IV curve is shifted by about +0.25 V, as can be seen in the inset of Fig. 5. Analogous measurements were performed on NDs of different diameters yielding qualitatively the same results, except that the data scatter increased with increasing diameter. The observed voltage shifts between the dark and the illuminated IV curves can be interpreted as the open circuit voltage of a photodetector or a solar cell and varies between ∼0.2 V and ∼0.4 V. In order to extract the serial resistance present in the system, the linear part of the negative branch of the dark IV curves has been fitted by a linear regression. The results are depicted in Fig. 6 as a function of the inverse square of the ND diameter. A progressive increase of the series resistance from ∼28 MΩ for 300 nm NDs to ∼50 MΩ for 80 nm NDs can be observed. The corresponding short circuit current I_{SC} at zero voltage is plotted as a function of the effective ND diameter in Fig. 7. Here, despite the large errors, a trend of increasing I_{SC} with increasing ND size is observable.

IV. DISCUSSION

In the following, we want to especially discuss the 2D current images recorded under different bias and illumination conditions. For Fig. 3(b), which was recorded under illumination by the SLD with 0 V sample bias, considerably high currents up to −5 nA appear preferentially at the transition regions between the {113} and {15 3 23} facets, whereas the {113} facets essentially exhibit no current. A comparison with

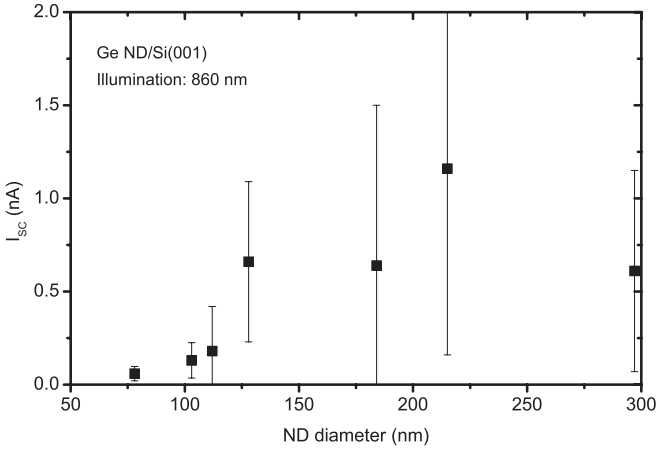

FIG. 7. Short circuit current I_{SC}, determined from IV curve analysis, as a function of the effective nanodome diameter.

Fig. 3(d), which was measured at the same position but without illumination, reveals that there is practically no current from the NDs in the dark. In this case, the surrounding wetting layer yields somewhat higher currents than the NDs. As can be seen from Fig. 3(d), the substrate current level is homogeneous at a level of about −7 pA. The slow scan direction was from top to bottom. These small currents are likely to be driven by a small offset of the voltage source.

The latter findings indicate that the currents measured in Fig. 3(b) are photogenerated. This is consistent with the dark and illuminated IV characteristics measured on top of individual NDs, as can be seen in Fig. 5. The IV characteristics at positive bias is dominated by the p-Si/Ag Schottky back contact, since this junction is forward biased for negative potentials and reversely biased for positive potentials at the Ag electrode. On the other hand, for the p-i-n diode formed between the p-silicon, the intrinsic SiGe NDs and the n-type diamond AFM tip forward, and the reverse direction is opposite to the back Schottky contact. The significant increase in the current for positive bias under illumination can be attributed to the photoinduced release of free charge carriers in the silicon. The back contact stays dark because the penetration depth of 860 nm radiation in crystalline silicon is just a few tens of micrometers. However, the minority carrier diffusion length is several 100 μm,[39] which means that photogenerated electrons can reach the back contact contributing to the increased current for positive potential at the back electrode. The shift of the IV curve, as shown in the inset of Fig. 5, is a clear indication for a photovoltage generation. The slight downward shift of the IV curve under illumination does not coincide with a photovoltage generated at the back contact. The photovoltage occurs due to spatial separation of photoexcited electron hole pairs in the build-in field of the space charge region. The decrease of the contact potential difference of the p-Si–GeND–n-diamond heterojunction under illumination provides the main contribution to the observed photovoltage. Obviously, the Ge ND on the p-silicon substrate forms a nanosize "solar cell" with the n-type (quasimetallic) diamond AFM tip as top electrode.

Parameters like the open circuit voltage V_{OC}, the short circuit current I_{SC}, and the serial resistance R_S can be extracted from the IV curves measured for different effective ND diameters. Comparing Figs. 6 and 7, it is obvious that the I_{SC} and the serial resistance follow opposite trends with ND size. While R_S decreases with increasing ND diameter, the I_{SC} exhibits an increase. This just resembles the dominance of the large serial resistance on the characteristics leading to a noticeable reduction of I_{SC}. A plot of R_S versus the inverse square of the effective ND diameter, as shown in Fig. 6, can be fitted acceptably well by a linear regression (full, black line in Fig. 6). This means that the measured resistance of a single ND is mainly determined by the ND-substrate interface area. Therefore, we can also conclude that possible compositional differences which go along with different ND sizes play a minor role in this size regime, at least as long as the ND is contacted at the top. The intersection of the regression line with the y axis yields a value of ∼27 MΩ, which represents the residual resistance not associated with the ND geometry. The main contribution to this high resistance is the contact between the AFM probe and the ND. First, there is certainly an oxide layer formed on the ND surface, which hinders current transport, and, second, the effective contact area between AFM tip and ND is just a few square nanometers, which also causes a significant resistance. For the V_{OC} values, no definitive trend with ND size could be found. The V_{OC} is a nonlinear function of the light intensity and should saturate for high intensities when the contact potential difference within the n-diamond–GeND–p-Si heterostructure is reached. For p-type silicon at the present doping level of $N_A \sim 10^{15}$ cm^{-3}, the work function is approximately 5 eV. The doping level and the work function of the nitrogen-doped diamond tip is not exactly known. In the literature, work function values equal to or smaller than 4.7 eV are given for single crystalline (100) diamond surfaces at doping concentrations of $N_D = 10^{20}$ cm^{-3} (Ref. 40). This yields a maximum V_{OC} of at least 0.3 V, which tolerably agrees with the measured values, suggesting that the SLD light causes a strong excitation.

A further interesting observation is the inhomogeneous distribution of current within a ND. For the unbiased case under illumination, the photocurrent maxima appear preferentially at the transition regions between the {113} and {15 3 23} facets, whereas the photocurrent is significantly reduced on the {113} facets. In contrast, a significant dark current at a sample bias of −0.5 V is also detectable on the {113} facets. As visible in Fig. 3(c) and the dark current profile in Fig. 4, there still is a variation in the conductivity across the NDs. However, since the dark current map is measured without feedback control, the contact forces vary significantly during the measurements. This affects the contact quality as well as the lateral resolution and therefore can lead to a different current profile. Conductivity variations within Ge NDs have been attributed to compositional inhomogeneities due to different Ge-Si intermixing during dot formation.[29] In this case—depending on the preparation conditions—current maxima were observed on the center region or the ND rim, which were thought to be Ge-rich regions. Also related to the local composition together with the formation of a surface oxide conductivity variations have been reported on InAs/GaAs quantum rings.[41] Other explanations have been stated for InAs quantum dots grown on n-GaAs substrates, which exhibited enhanced conductivity in the dot center region. There, the observation was explained in terms of surface state associated local surface band bending, which lowers the Schottky barrier between quantum dot and AFM tip.[42] For this system, a strongly reduced conductivity of the wetting layer was also observed. This was attributed to Fermi-level pinning due to surface states in conjunction with the nanosize contact formed between AFM tip and surface. Compositional inhomogeneities within SiGe NDs were also found via selective etching experiments and subsequent AFM topography investigations.[43,44] Ge domes prepared at 600° C showed in general a ringlike increase of silicon content along the ND rim. In addition, protrusions along the ring indicated areas with even higher Si concentration along the ring. These areas of high Si concentration can be found close to the positions of the {113} facets, which can explain the local reduction in conductivity observed here. It should also be taken into account that the different facets will in general exhibit different work functions, irrespective of their composition, which yields different contact properties. The

latter possible influences on the local conductivity are hard to separate because they are not independent from each other. Facets of different crystallographic orientation will in general exhibit different surface atom densities, structures, and reconstructions, which yield different work functions but also different oxidation rates. However, both quantities are also strongly influenced by surface composition. Facets with higher surface atom density usually exhibit a higher rate of oxidation especially at low temperatures.[45,46] The oxidation properties change dramatically in silicon germanium mixtures, where Si is preferentially oxidized.[47,48] A clear separation of all contributing effects would need additional investigations on the details of facet structure, orientation, and composition-dependent oxidation behavior as well as on the work function, which lies beyond the scope of this work. Additionally, it has been shown that native oxides in this system do not cause qualitative changes in the current distribution within a dome.[30] Therefore, it is rational to attribute the changes in conductivity mainly to local changes in the Si concentration.

The almost insulating behavior of the wetting layer is a further surprising result because the residual layer usually also contains large amounts of Ge.[49] However, the C-AFM experiments were performed under ambient conditions, thus oxide formation has to be considered as well. It has been shown that native oxide influences the I–V characteristics measured at the center of individual Ge nanodots but has no qualitative influence on the measured current distribution within a dot.[30] For SiGe alloys, a strong oxidation of Si is reported whereas the Ge remains unchanged.[45] This has been explained by Ge catalyzed oxidation of Si, where the oxidized Ge is reduced by the silicon.[46] Formation of mixed oxides sets in when the silicon supply to the SiO_2/SiGe interface is insufficient. Moreover, the Si oxidation rate is accelerated by the presence of Ge promoting a fast growth of a SiO_2 layer. This can in fact explain the low conductivity of the wetting layer between the dome islands. Since there is effectively unlimited silicon supply from the substrate, the surface between the NDs will mainly be composed of SiO_2. Silicon oxide is an excellent electric insulator and inhibits charge transport effectively. The very small dark currents in the pA-range are most probably just creepage currents induced by a small offset of the voltage source and transported through the adsorbed water layer, which is always present on SiO_2 under ambient conditions.

V. SUMMARY/CONCLUSION

In this work, we investigated the morphological and electrical properties of individual Ge nanoislands on Si(001) with C-AFM and PC-AFM under ambient conditions. Intermittent contact mode topography images of the MBE grown samples revealed NDs with pronounced {113} and {15 3 23} facets. The majority of the NDs had effective diameters larger than 100 nm. 2D current maps recorded under illumination and in the dark revealed an inhomogeneous current distribution over the NDs. The current maxima mainly appeared at the transition between the {113} and {15 3 23} facets, whereas the {113} facets appeared least conductive. This inhomogeneous current distribution has mainly been attributed to local Si enrichment near these facets. The current-to-voltage characteristics measured at the center of individual NDs was governed by the Ag/Si back Schottky contact. The main contribution of the NDs is an additional serial resistance that scales with the ND-substrate interface area. Most importantly, it could be shown that a photovoltage is generated in the *p-i-n* structure formed by the *p*-type substrate, the Ge ND, and the *n*-type diamond AFM tip. The low conductivity of the ND free wetting layer was attributed to the Ge catalyzed formation of a SiO_2 layer that effectively hinders current flow. Future experiments employing Kelvin probe force microscopy measurements under controlled environment will provide further information about the local work function of the different ND facets. Comparison of KPFM and C-AFM measurements on etched and unmodified samples will also elucidate the role of oxidation on the electrical properties of NDs and wetting layer.

ACKNOWLEDGMENTS

We gratefully acknowledge the financial support within the bilateral Project UA 11/2009 of the Austrian Academic Exchange Service and the Project No. P19636-N20 of the Austrian Research Fund (FWF). In addition, we are thankful for the financial support by the program of fundamental research of the National Academy of Sciences of Ukraine, Nanostructured Systems, Nanomaterials, Nanotechnologies within Project No. 9/07 and Project No. M/34-09 by the Ministry of Education and Science of Ukraine. We also acknowledge the fruitful discussion with Prof. G. Bauer, Linz.

*teichert@unileoben.ac.at

[1]Edited by O. G. Schmidt, *Lateral Alignment of Epitaxial Quantum Dots* (Springer-Verlag, Berlin, Heidelberg, 2007).

[2]C. Teichert, Phys. Rep. **365**, 335 (2002).

[3]K. Brunner, Rep. Prog. Phys. **65**, 27 (2002).

[4]G. Costantini, A. Rastelli, C. Manzano, R. Songmuang, O. G. Schmidt, K. Kern, and H. von Kanel, Appl. Phys. Lett. **85**, 5673 (2004).

[5]R. Gatti, F. Pezzoli, F. Boioli, F. Montalenti, and L. Miglio, J. Phys.: Condens. Matter **24**, 104018 (2012).

[6]T. I. Kamins, G. Medeiros-Ribeiro, D. A. A. Ohlberg, and R. S. Williams, J. Appl. Phys. **85**, 1159 (1999).

[7]M. Lutz, R. Feenstra, P. Mooney, J. Tersoff, and J. Chu, Surf. Sci. **316**, L1075 (1994).

[8]Y.-W. Mo, D. E. Savage, B. S. Swartzentruber, and M. G. Lagally, Phys. Rev. Lett. **65**, 1020 (1990).

[9]P. Sutter, E. Mateeva-Sutter, and L. Vescan, Appl. Phys. Lett. **78**, 1736 (2001).

[10]E. Kasper and D. Paul, *Silicon Quantum Integrated Cicuits: Silicon-Germanium Heterostructure Devices: Basics and Realisation* (Springer, Berlin, Heidelberg, 2010).

[11]O. E. Schmidt and K. Eberl, IEEE Trans. Electron Devices **48**, 1175 (2001).

[12]E. Kasper, Appl. Surf. Sci. **102**, 189 (1996).

[13]J. Suh, R. Nakane, N. Taoka, M. Takenaka, and S. Takagi, Appl. Phys. Lett. **99**, 142108 (2011).
[14]J. Oh, J. Huang, I. Ok, S. H. Lee, P. D. Kirsch, R. Jammy, and H. D. Lee, IEICE Trans. Electronics **E94C**, 712 (2011).
[15]P. Rauter, T. Fromherz, C. Falub, D. Grutzmacher, and G. Bauer, Appl. Phys. Lett. **94**, 081115 (2009).
[16]M. Kolahdouz, A. A. Farniya, L. Di Benedetto, and H. H. Radamson, Appl. Phys. Lett. **96**, 213516 (2010).
[17]V. A. Shchukin, N. N. Ledentsov, P. S. Kopev, and D. Bimberg, Phys. Rev. Lett. **75**, 2968 (1995).
[18]J. H. Zhu, K. Brunner, G. Abstreiter, O. Kienzle, and F. Ernst, Thin Solid Films **336**, 252 (1998).
[19]F. Liu, A. H. Li, and M. G. Lagally, Phys. Rev. Lett. **87**, 126103 (2001).
[20]J. Tersoff, C. Teichert, and M. G. Lagally, Phys. Rev. Lett. **76**, 1675 (1996).
[21]Z. Y. Zhong, G. Chen, J. Stangl, T. Fromherz, F. Schaffler, and G. Bauer, Physica E **21**, 588 (2004).
[22]C. Teichert, M. G. Lagally, L. J. Peticolas, J. C. Bean, and J. Tersoff, Phys. Rev. B **53**, 16334 (1996).
[23]E. Mateeva, P. Sutter, J. C. Bean, and M. G. Lagally, Appl. Phys. Lett. **71**, 3233 (1997).
[24]J. Novak, V. Holy, J. Stangl, T. Fromherz, Z. Zhong, G. Chen, G. Bauer, and B. Struth, J. Appl. Phys. **98**, 073517 (2005).
[25]V. S. Lysenko, Y. V. Gomeniuk, V. V. Strelchuk, A. S. Nikolenko, S. V. Kondratenko, Y. N. Kozyrev, M. Y. Rubezhanska, and C. Teichert, Phys. Rev. B **84**, 115425 (2011).
[26]C. H. Lin, C. Y. Yu, C. C. Chang, C. H. Lee, Y. J. Yang, W. S. Ho, Y. Y. Chen, M. H. Liao, C. T. Cho, C. Y. Peng, and C. W. Liu, IEEE Trans. Nanotechnol. **7**, 558 (2008).
[27]T. I. Kamins, K. Nauka, and R. S. Williams, Appl. Phys. A **73**, 1 (2001).
[28]F. Xue, J. Qin, J. Cui, Y. Fan, Z. Jiang, and X. Yang, Surf. Sci. **592**, 65 (2005).
[29]R. Wu, F. H. Li, Z. M. Jiang, and X. Yang, Nanotechnology **17**, 5111 (2006).
[30]Z. Lin, P. Brunkov, F. Bassani, and G. Bremond, Appl. Phys. Lett. **97**, 263112 (2010).
[31]H.-C. Chung, W.-H. Chu, and C.-P. Liu, Appl. Phys. Lett. **89**, 82105 (2006).
[32]A. Olbrich, B. Ebersberger, and C. Boit, Appl. Phys. Lett. **73**, 3114 (1998).
[33]C. Teichert and I. Beinik, in *Scanning Probe Microscopy in Nanoscience and Nanotechnology*, Vol. 2 (Springer, Berlin, 2011), p. 691.
[34]S. Kremmer, S. Peissl, C. Teichert, F. Kuchar, and H. Hofer, Mater. Sci. Eng. B **102**, 88 (2003).
[35]H. Sakaguchi, F. Iwata, A. Hirai, A. Sasaki, and T. Nagamura, Jpn. J. Appl. Phys. **38**, 3908 (1999).
[36]Y. Kozyrev, S. Kondratenko, M. Rubezhanska, V. Lysenko, C. Teichert, and C. Hofer, in *Nanomaterials and Supramolecular-Structure Physics, Chemistry and Applications* (Springer, Berlin, 2010), p. 235.
[37]Gwyddion 2.28.20120524 an SPM data and visualization and analysis tool, D. Nečas, P. Klapetek, C. Anderson, M. Šiler, J. Bílek, N. Ocelic, R. Zitko, L. Chvátal, S. Neumann, J. Hořák, A. Kowalev, O. Davies, R. Würdemann, D. Kähler, M. Valtr, M. Hasoň, P. Rahe, M. Caldwell, A. Gruzdev, D. Bratašov, F. Bianco, L. Somers, V. Salajka, A. Campbellova and L. Fricke (Czech Metrology Institute, 2012), http://gwyddion.net/.
[38]S. Sze and K. N. Kwok, *Physics of Semiconductor Devices*, 3 ed. (John Wiley & Sons, Inc., Hoboken, 2007).
[39]L. Diederich, O. Kuettel, P. Aebi, and L. Schlapbach, Surf. Sci. **418**, 219 (1998).
[40]T. Mlaklar, G. Biasiol, S. Heun, L. Sorba, T. Vijaykumar, G. Kulkarni, V. Spreafico, and S. Prato, Appl. Phys. Lett. **92**, 192105 (2008).
[41]I. Tanaka, I. Kamiya, H. Sakaki, N. Quershi, S. Allen, Jr., and P. Petroff, Appl. Phys. Lett. **74**, 844 (1999).
[42]K. Georgios, Ph.D. Thesis, University of Konstanz, Germany, 2006.
[43]G. Katsaros, M. Stoffel, A. Rastelli, O. G. Schmidt, K. Kern, and J. Tersoff, Appl. Phys. Lett. **91**, 013112 (2007).
[44]E. A. Lewis and E. A. Irene, J. Electrochem. Soc. **134**, 2332 (1987).
[45]J. Sladkova, Czech. J. Phys. B **27**, 943 (1977).
[46]F. LeGoues, R. Rosenberg, T. Nguyen, F. Himpsel, and B. Meyerson, J. Appl. Phys. **65**, 1724 (1989).
[47]P. Hellberg, S.-L. Zhang, F. d'Heurl, and C. Petersson, J. Appl. Phys. **82**, 5779 (1997).
[48]M. Brehm, M. Grydlik, H. Groiss, F. Hackl, F. Schäffler, T. Fromherz, and G. Bauer, J. Appl. Phys. **109**, 123505 (2011).
[49]M. Brehm, M. Grydlik, H. Lichtenberger, T. Fromherz, N. Hrauda, W. Jantsch, F. Schaffler, and G. Bauer, Appl. Phys. Lett. **93**, 121901 (2008).